coatings

MDPI

Article

A Novel Oxide Layer Formed on the 800 °C-Annealed CoMoCrSi Coating Significantly Reduced Friction and Wear at Room Temperature

Hongjian Guo [1,2], Bo Li [3,*], Pengxun Yan [2,*] and Zhiguo Wu [2]

1 School of Bailie Mechanical Engineering, Lanzhou City University, Lanzhou 730070, China; guohj@lzcu.edu.cn
2 Institute of Nanomaterials Application Technology, Gansu Academy of Sciences, Lanzhou 730000, China; zgwu@lzu.edu.cn
3 State Key Laboratory for Mechanical Behaviour of Materials, School of Materials Science and Engineering, Xi'an Jiaotong University, Xi'an 710049, China
* Correspondence: libo616@mail.xjtu.edu.cn (B.L.); pxyan@lzu.edu.cn (P.Y.)

Abstract: In the present work, we investigated the microstructures and properties of as-sprayed and annealed CoMoCrSi coatings. Specifically, the annealed treatment at 800 °C resulted in good recrystallization, improved microstructure, and enhanced properties of CoMoCrSi coatings. An oxide layer formed on the annealed coating surfaces; it was mainly composed of nano-sized Cr_2O_3 and micro-sized $CoMoO_4$, and could account for the increased surface microhardness and enhanced anti-wear performance of annealed coatings. In particular, the very hard Cr_2O_3 played a critical role of resisting press-in and wear during the tests, and the $CoMoO_4$ had a lubricating effect during the friction process. Finally, the annealed coatings exhibited low coefficients of friction (COFs) of 0.4 and wear rates of 0.7–0.8 $\times$ 10^{-6} $mm^3 \cdot N^{-1} \cdot m^{-1}$ after a long sliding distance of 1000 m at RT. Consequently, the wear mechanism transferred from brittle fracture coupled with abrasive wear for the as-sprayed coating to slight abrasive wear for annealed coatings.

Keywords: annealed treatment; CoMoCrSi coating; oxides layer; tribological performance

Citation: Guo, H.; Li, B.; Yan, P.; Wu, Z. A Novel Oxide Layer Formed on the 800 °C-Annealed CoMoCrSi Coating Significantly Reduced Friction and Wear at Room Temperature. *Coatings* **2021**, *11*, 290. https://doi.org/10.3390/coatings11030290

Academic Editor: Joe Sakai

Received: 9 February 2021
Accepted: 26 February 2021
Published: 3 March 2021

1. Introduction

Thermally sprayed coatings have been widely applied to provide necessary protection against oxidation, wear, and corrosion in various industrial fields, e.g., the traditional machinery industries (gears, rollers, valves, bearings, wheels, axles, and drills), ocean engineering, and aerospace industries [1–10]. They are also a low-cost, effective way to enhance the surface properties and to prolong the service life of related mechanical parts. Many types of thermal spraying techniques have been developed, including oxygen-acetylene flame spraying, low voltage plasma spraying, atmospheric plasma spraying (APS), cold spraying, arc spraying, high-velocity oxygen fuel (HVOF) spraying, and high-velocity air spraying. Compared with other spraying techniques, HVOF technology [11,12] is usually utilized to fabricate alloy coatings due to its much lower temperature, higher particle velocity, and less in-flight time, and to obtain compact and less oxidized coatings.

The Co-based alloys, as a branch of Tribaloy alloys, have been widely applied in various harsh conditions due to their superior hardness and excellent wear performance as well as their high corrosion resistance. The Co Tribaloy alloy (similar to T-800) (8.5% Mo-17.5% Cr-3.4% Si) has a hardness of up to 1000–1200 HV because of hard ternary Laves phase, e.g., Co_3Mo_2Si or CoMoSi [13]. In addition, Mo and Si in the alloy can improve the high temperature strength and wear performance of the alloy, and Cr contributes to high oxidation resistance by means of the formation of Cr_2O_3 layer [14,15]. However, recent studies [16–18] showed that CoMoCrSi coatings usually exhibited an amorphous microstructure, which resulted in brittle and low plastic performance at room temperature

(RT). Moreover, the sprayed CoMoCrSi coatings, especially prepared by ordinary flame or APS techniques, normally possessed inescapable defects, e.g., pores, cracks, and inclusions, which caused looser structures and lower mechanical performance compared to the corresponding alloy. It has been well verified that annealed treatment could effectively enhance the mechanical wear and oxidation properties of the coatings [19–22]. As for the investigations concerning the annealed CoMoCrSi alloy coatings, a study revealed that the cavitation damage of APS-sprayed CoMoCrSi coatings could be significantly alleviated after heat treatment at 1000 °C [23]. Although the HVOF-sprayed CoMoCrSi alloy coatings were annealed at 200, 400, and 600 °C for 1 h [12,24], heat treatments at 200 and 400 °C did not cause any major change in microstructures and wear properties. The 600 °C heat treatment caused a slight crystallization with the formation of sub-micrometric crystalline regions, resulting in a definite hardness increase and reduction of wear rate at room temperature. This result is not ideal. Recently, a report [25] indicated that annealing treatment at 600 and 1000 °C could lead to the phase transformation, and improvement in mechanical and tribological properties of the APS-sprayed CoMoCrSi coating. However, the structure of the coating, that is the oxides formed on the coating surface after heat treatment, and its influence on the performance of the coating were not deeply analyzed. We have evaluated the tribological properties of the HVOF-sprayed CoMoCrSi coatings in a wide temperature range (from RT to 800 °C) [18]. The result demonstrated that the as-sprayed coatings registered an excellent tribological performance up to 600 and 800 °C, and unsatisfactory wear properties at low temperatures. Occasionally, we found that numerous Cr_2O_3 and $CoMoO_4$ particles dispersively distributed on the coating surface after wear at 800 °C, implying oxidation occurred during the process of heating up and the friction test. There was also a report [12] that the differential thermal analysis and thermal gravimetric analysis (DTA-TG) result of Co-based alloy powder displayed an obvious exothermal peak as the temperature increased to 812 °C, indicating the oxidation of the powder. Considering the discontinuous particles on the coating surface, which might be due to short time under 800 °C, we intended to anneal the as-sprayed CoMoCrSi coating at 800 °C and prolong the annealing time to 3, 5, and 10 h, to improve the tribological properties of CoMoCrSi coating at room temperature.

In the current work, we investigated the following: (a) the microstructure and phase transformation of CoMoCrSi coatings before and after annealed treatment, (b) the influence of oxide formation on the mechanical and tribological properties of CoMoCrSi coatings at RT, and (c) the wear mechanisms of CoMoCrSi coatings.

2. Materials and Methods

2.1. Coatings Fabrication

A type of commercial CoMoCrSi powder (Metco Diamalloy 3001, Winterthur, Switzerland) was used for feedstock, the surface morphology SEM image of which is shown in Figure 1; the powder particles were spherical and sized below 30 μm. Moreover, energy dispersive x-ray spectroscopic (EDS) investigation (insert in Figure 1) basically agreed with the nominal chemical composition of the CoMoCrSi powder. Diamond Jet 2700 HVOF spraying equipment (Sulzer Metco, NewYork, NY, USA) manipulated with an IRB 2400/16 robot (ABB, Vesteros, Switzerland) was used to fabricate the CoMoCrSi coatings, and the major spraying parameters are as follows: oxygen flow of 21.06 $m^3 \cdot h^{-1}$, natural gas flow of 13.14 $m^3 \cdot h^{-1}$, nitrogen flow of 18.7 $m^3 \cdot h^{-1}$, and spray distance of 27 mm; the concrete details have been reported elsewhere [18]. The substrate was 316L stainless steel. The substrates were ultrasonically cleaned in a mixture of alcohol and acetone for 20 min after the alloys were machined to target size (Φ20 mm × 10 mm for the friction tests and 25 mm × 20 mm × 10 mm for the microstructure observation) and sandblasted. The specific chemical compositions of CoMoCrSi coating and 316L steel are presented in Table 1.

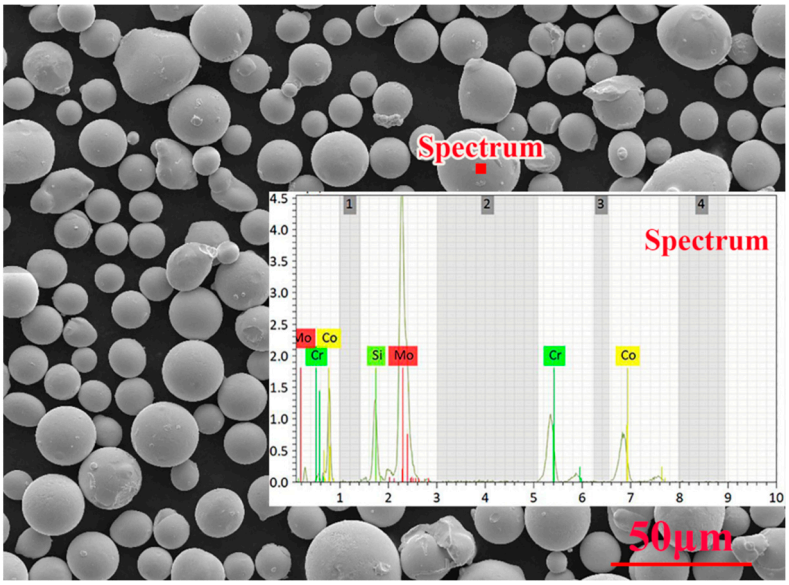

Figure 1. Surface morphology and EDS result of the CoMoCrSi powder.

Table 1. Chemical composition of CoMoCrSi coating and 316L steel.

Items	Elements w.t.%							
	Co	**Mo**	**Cr**	**Si**	**Ni**	**Mn**	**P**	**S**
CoMoCrSi coating	50.6	28.5	17.5	3.4	–	–	–	–
316L steel	–	2.0–3.0	16.0–18.0	≤1.0	12.0–15.0	≤2.0	≤0.035	≤0.030

2.2. Isothermal Oxidation

Isothermal oxidation of the coating was carried out at 800 °C in a muffle furnace with a heating rate of 5 °C·min^{-1} and held there for 3 h, 5 h, and 10 h, respectively. The specimens were naturally cooled in the muffle furnace.

2.3. Characterization of Coatings

Microstructures and wear tracks of coatings were characterized by using a scanning electron microscope (TESCAN MIRA3 Bron, Kohoutovice, Czech Republic) with an energy dispersive X-ray spectrometry (EDS, Bruker, Leipzig, Germany). The phase composition of the coatings before and after the annealing treatment was evaluated by X-ray diffraction (Rigaku D/max-RB, λ = 0.15 nm, Tokyo, Japan); the specific operation parameters have been reported in previous work. Jade 6.5 software (TILAB) based on the standard ICSD pattern (51/54529) data files was used to analyze the XRD results.

Indentation tests were carried out by an MH-5-VM microhardness tester (Shanghai Hengyi Science and Technology Corporation, Shanghai, China) with a load of 300 g and dwelling time of 10 s. In particular, the surface microhardness was randomly evaluated on the coating surface, and an average of ten measured values was reported as the final result, which was also applied to the report of the cross-sectional microhardness. Moreover, the cross-sectional hardness was measured from the substrate to coating cross-section.

A ball-on-disc tribometer (CSM, Locarno, Switzerland) was employed to assess the tribological performance of the coatings at room temperature (RT) (about 25 ± 5 °C). Al_2O_3 balls with a diameter of 6 mm were used as the counterpart. All tests were carried out under normal load of 5 N, line velocity of 10 cm·s^{-1}, rotating radius of 5 mm, and sliding distance of 1000 m. The tests were performed on three specimens annealed at the same temperature to reduce the error, and the average of the three measured COF values were reported as the final result. A two-dimensional surface profiler (KLA-tencor D-100, KLA-Tencor, Silicon Valley, CA, USA) was employed to measure the volume loss of the coatings after the friction

tests. It is notable that the volume loss of each specimen was measured at three different spots, and the final volume loss value was the average of nine measured values obtained from the three specimens. Subsequently, the wear rates of coatings (K_W, $mm^3 \cdot N^{-1} \cdot m^{-1}$) were obtained based on an equation, $K_W = V_W/(P \times L)$, as reported previously, where V_W is the wear volume loss in mm^3, P is the normal load applied in newton (N), and L is the sliding distance in meter (m). The average of five measurements is reported as the final result. The Horiba Raman microscope (Jobin Yvon, France) with 532 nm He–Ne laser was used to analyze the phase composition of the coating surface and wear track, and conducted in the range of 100 to 1500 cm^{-1}.

3. Results and Discussion

3.1. Microstructure of the Coatings

Figure 2 shows X-ray diffraction patterns of as-sprayed and annealed CoMoCrSi coatings. The as-sprayed coating displayed a wide peak at 43.6°, which implies amorphous phases made up the coating. Additionally, some hard intermetallic phases, such as Co_7Mo_6 (PDF#29-0489) and Co_3Mo_2Si (PDF#30-0449) [12,24], could be detected in this coating. However, the annealed CoMoCrSi coatings exhibited well-crystallized structures after heat treatment, demonstrating recrystallization and oxidation occurred during the process. In particular, the diffuse scattering peak disappeared, and numerous diffraction peaks represented new metal oxides appeared in the patterns of annealed coatings. Those pointed diffraction peaks could be identified as metal oxides and bimetallic oxides including Cr_2O_3 (PDF#38-1479), Co_3O_4 (PDF#43-1003), $CoMoO_4$ (PDF#25-1434), Co_7Mo_6 and Co_3Mo_2Si [25–27]. Moreover, the phase composition of the annealed coatings changed slightly when the annealing time was prolonged. The number and intensity of the $CoMoO_4$ peaks decreased when the annealing time increasing from 3 h to 10 h, especially in the diffraction angle range of 25° to 30°, while the $CoMoO_4$ peaks disappeared in the patterns of coating annealed for 10 h, implying that the volume fraction of $CoMoO_4$ phase reduced. On the contrary, the intensity of Cr_2O_3 peaks increased with increase in annealing time, indicating that the volume fraction and grain size of Cr_2O_3 phase increased [25].

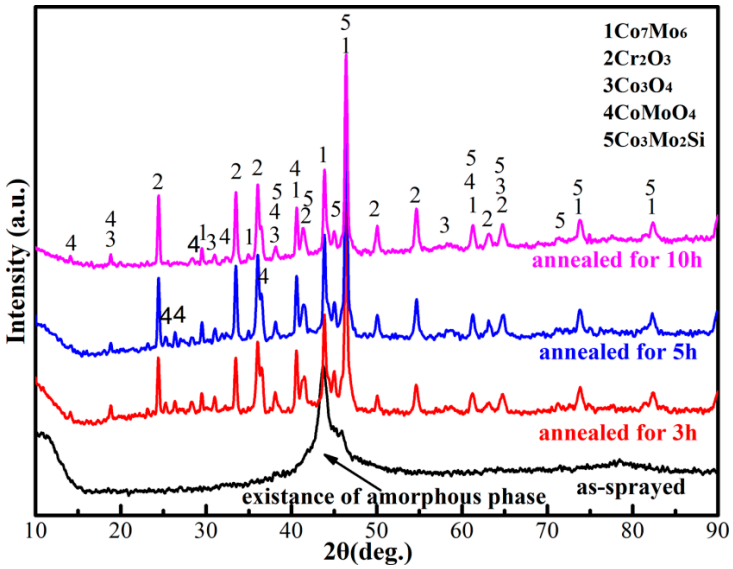

Figure 2. X-ray diffraction patterns of as-sprayed and annealed CoMoCrSi coating.

To further investigate the oxidation after heat treatment, surface morphologies of as-sprayed and annealed coatings are demonstrated in Figure 3. In particular, Figure 3a,b displays the polished surface of as-sprayed coating, which exhibits compact microstructure except for a few unfused particles and micropores. Moreover, grain boundaries and compact structures can be clearly seen in the highly magnified image (as indicated in

Figure 3b). However, annealed coatings possess different surface morphologies compared to the as-sprayed coatings. Specifically, numerous light-white island structures were distributed on the grey surface of annealed coatings (Figure 3c,e,g). The number of these reduced as the annealing time increased from 3 h to 10 h. According to the highly magnified images (Figure 3d,f,h), the dark grey areas were composed of a great number of nano-sized (300–500 nm) olivine-shaped particles, and the light-white islands were made up of numerous micron-sized (1–4 μm) pomegranate-seed-like particles. Furthermore, EDS analyses were conducted on the corresponding spots (as indicated in Figure 3d,f,g) and the atomic ratios of the elements are itemized in Table 2. In combination with above results of XRD analysis, the dark grey particles were identified as Cr_2O_3, and the light-white islands as $CoMoO_4$ (as indicated in Figure 3). This verifies the XRD result that the quantity of $CoMoO_4$ decreased with increase in annealing time.

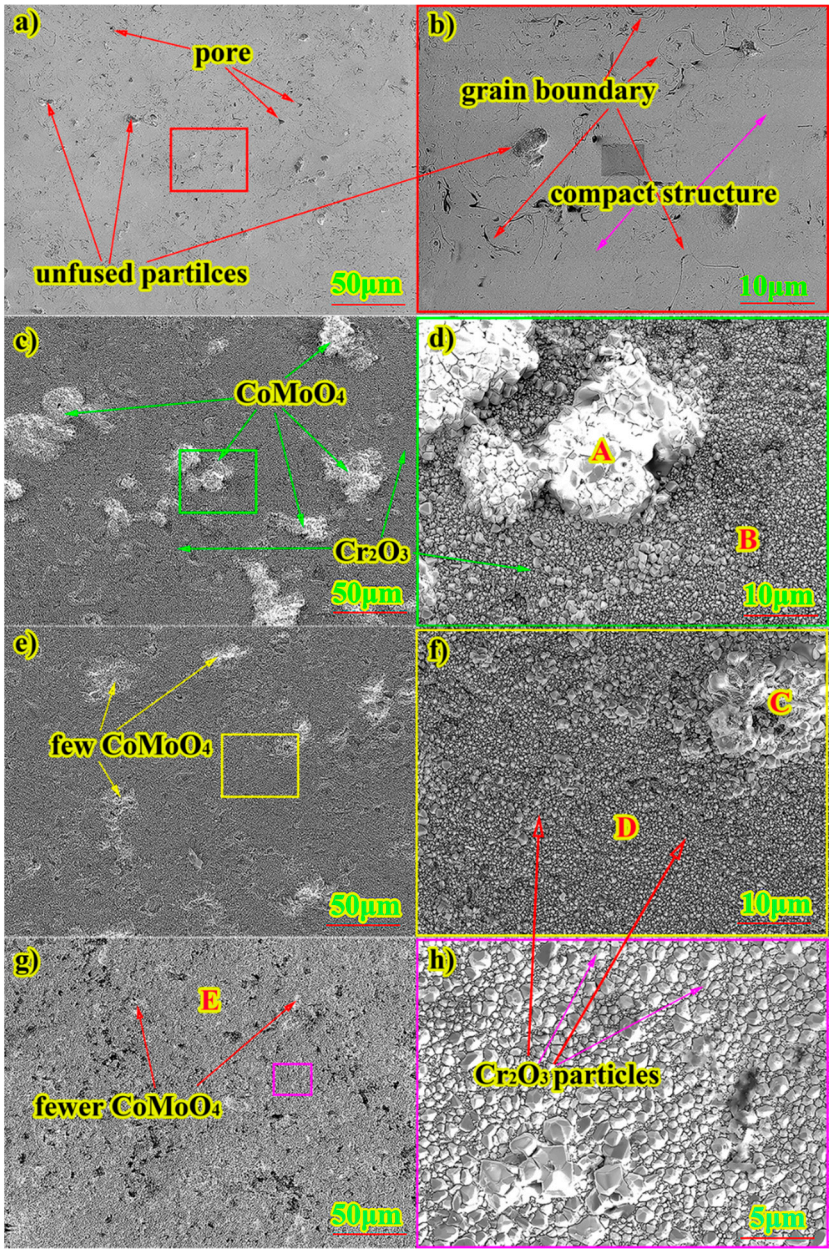

Figure 3. Surface SEM images of as-sprayed CoMoCrSi coating (**a**,**b**) and coatings annealed for 3 h (**c**,**d**), 5 h (**e**,**f**), and 10 h (**g**,**h**).

Table 2. EDS results of different spots indicated in Figure 3d,f,g.

Spots	Elements At.%					Demonstration
	Co	Mo	Cr	Si	O	
A	20.14	17.05	4.06	0.2	68.75	$CoMoO_4$
B	8.27	1.19	36.20	0.41	53.93	Cr_2O_3
C	21.65	15.87	2.58	0.13	59.77	$CoMoO_4$
D	8.89	1.03	38.10	0.35	52.53	Cr_2O_3
E	5.06	0.86	39.95	0.16	53.97	Cr_2O_3

Figure 4 illustrates the cross-sectional morphologies of as-sprayed and annealed CoMoCrSi coatings. All the SEM images were obtained with a magnification of 5000 × from the coating cross-sections. It can be seen that, except for a few pores, layered and compact structures make up the as-sprayed CoMoCrSi coating (Figure 4a). Moreover, the annealed coatings show different morphologies after annealing treatment. In particular, grain boundaries are obvious, and a great number of precipitated phases with spherical and irregular shape were distributed in layered structures (as indicated in Figure 4). According to the EDS result (Figure 5), the Cr and O elements are rich in these precipitated phases regions, and the Co, Mo, and Cr elements are homogenously distributed in the compact areas. This could be attributed to recrystallization of phases during the process of annealing treatment, as well as the fact that some chromium oxide (not necessarily Cr_2O_3) grains formed and gathered at the boundaries of layered structures. As a whole, the coating structures can be significantly improved after heat treatment at 800 °C.

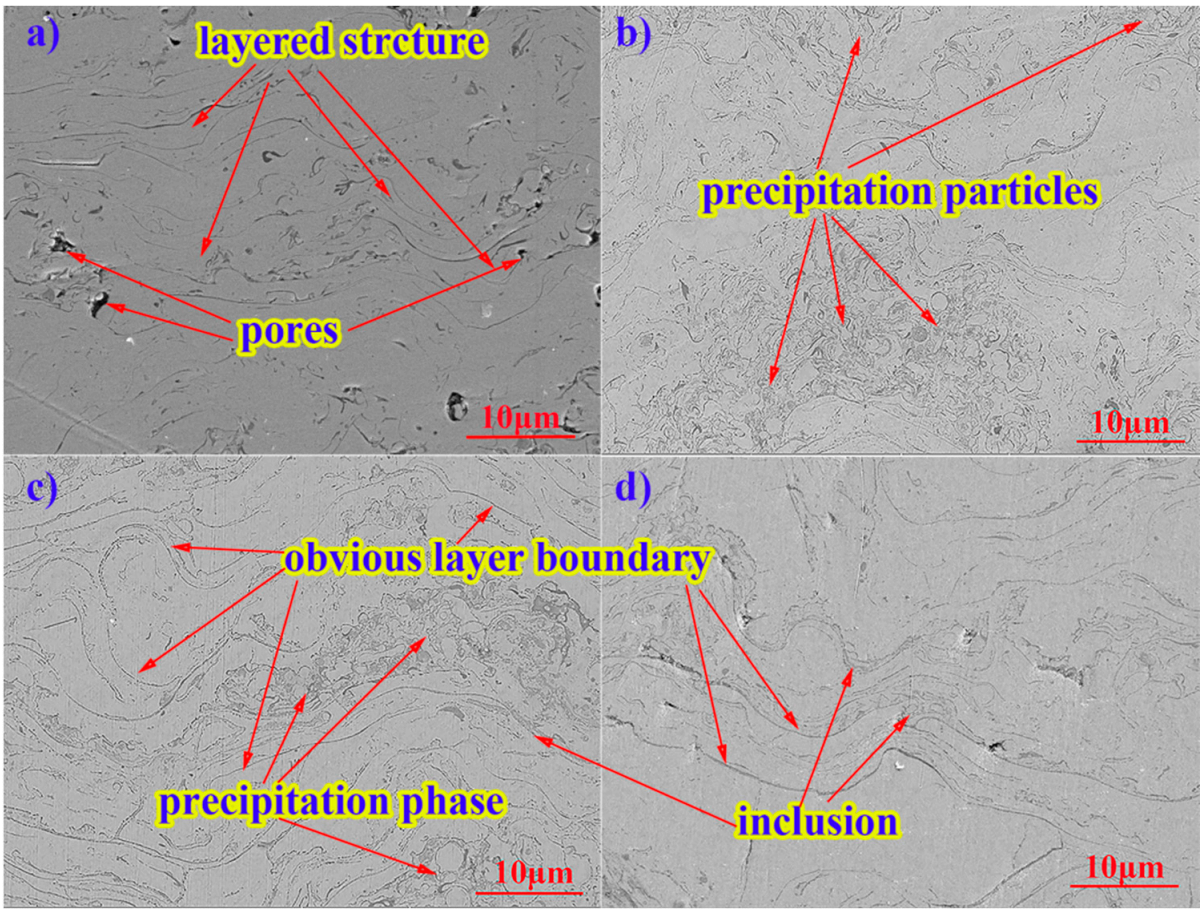

Figure 4. Cross-sectional images of as-sprayed CoMoCrSi coating (**a**) and coatings annealed for 3 h (**b**), 5 h (**c**), and 10 h (**d**).

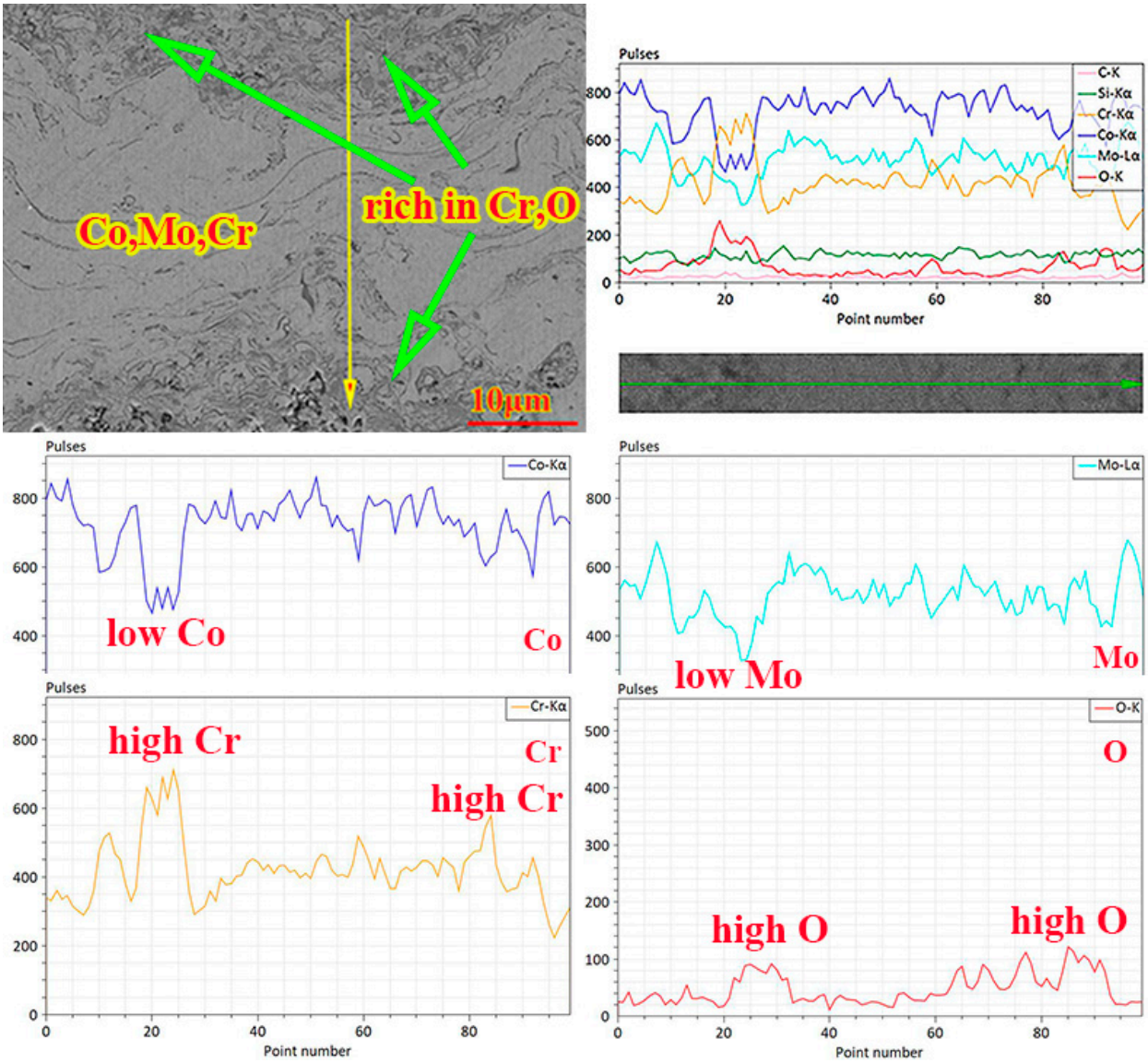

Figure 5. Linear scanning result of cross-section of coating annealed for 5 h.

3.2. Microhardness of the Coatings

Hardness is a symbol of anti-wear resistance of the coatings. Thus, microhardness values of as-sprayed and annealed coatings are measured and illustrated Figure 6. In particular, the annealed coatings registered a higher micro-hardness than the as-sprayed coating (Figure 6a), the surface microhardness was higher than the cross-sectional microhardness for all coatings, which is consistent to the other reports [12,25]. In brief, the surface microhardness increased from 902.8 $HV_{0.3}$ to 1257.9 $HV_{0.3}$ after the heat treatment at 800 °C for 10 h (increased by 40%), and the cross-sectional microhardness was up to 965.6 $HV_{0.3}$. The results are better than the reported CoMoCrSi coatings (550–650 $HV_{0.3}$) [17], and even comparable to the HVOF-sprayed CoMoCrSi-Cr3C2 coating elsewhere [28]. In addition, the variations of cross-sectional microhardness from substrates to the coatings are depicted in Figure 6b. There were obvious differences between the microhardness of the coatings and substrates, however, the microhardness across the thickness of coatings was not remarkably different for every specimen (as shown in Figure 6b), indicating the balanced mechanical property of the coatings.

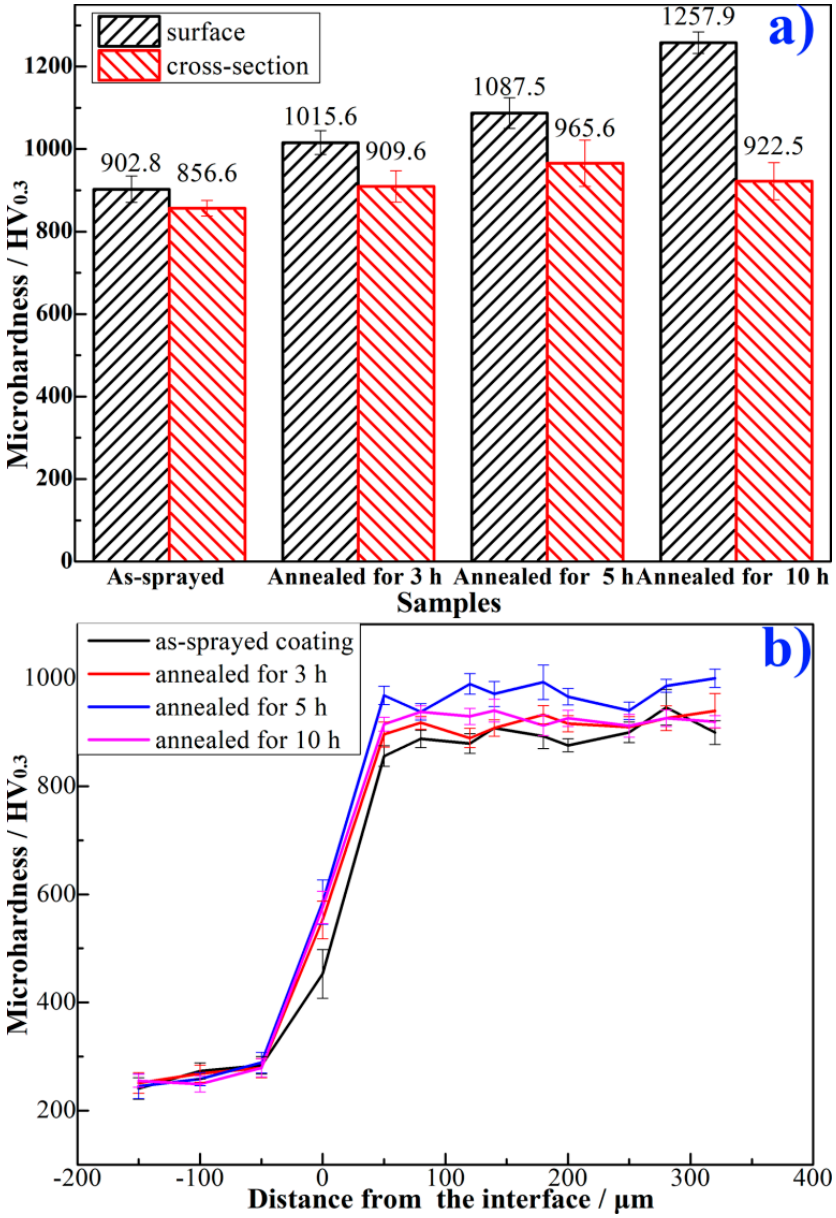

Figure 6. Average microhardness of the CoMoCrSi coatings (**a**) and variation across the thickness (**b**).

Figure 7 displays the indentation morphologies of as-sprayed and annealed CoMoCrSi coatings. It can be clearly seen that the area of the indentation gradually reduced with the annealing time increased, which demonstrates the increasing of microhardness value. Furthermore, the indentation morphology of as-sprayed coating implies that the brittle crack occurred after the test (Figure 7a). However, the plastic deformation could be verified by the indentation morphology of coating annealed for 5 h (as indicated in insert in Figure 7c), where wave-like patterns are obvious on the regular indentation surface. Although some tiny malleable cracks can be found around the indentation (Figure 7c,d), it could be concluded that toughness and plasticity of annealed coatings had been improved after annealed treatment.

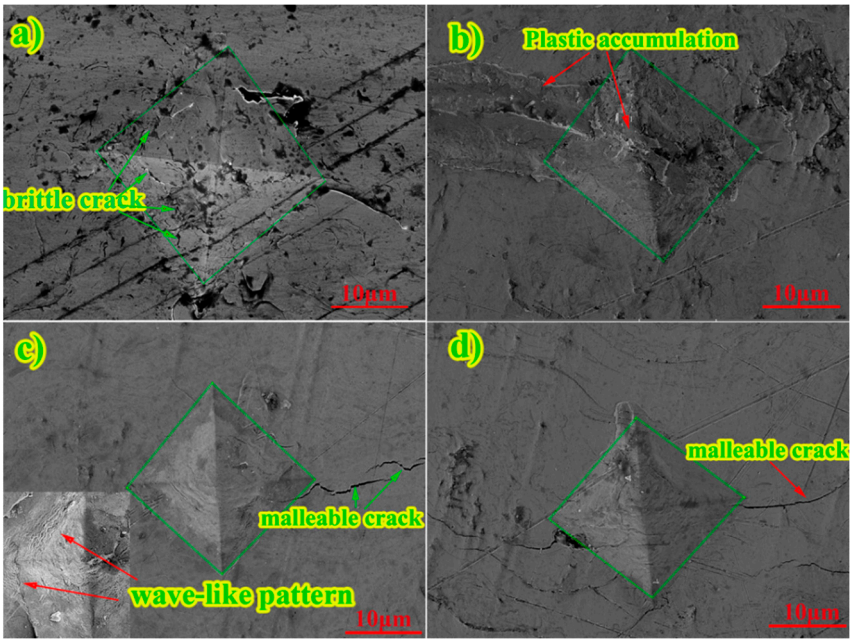

Figure 7. Indentation morphologies of as-sprayed CoMoCrSi coating (**a**) and coating annealed for 3 h (**b**), 5 h (**c**), and 10 h (**d**).

3.3. Tribological Performance of the Coatings

To evaluate the influence of oxidation on the tribological performance, friction tests were carried out on as-sprayed and annealed CoMoCrSi coatings with a long sliding distance of 1000 m. The friction coefficient–distance curves are illustrated in Figure 8. It is obvious that the coefficient of friction (COF) of the as-sprayed coating is higher than that of annealed coatings. In particular, the as-sprayed coating registered a COF of 0.53 in the first 120 m, however, the COF increased and stabilized at 0.79 for the remaining distance. Moreover, the coating annealed for 3 h exhibited the lowest COF in the range of 0.36 to 0.39, the coatings annealed for 5 h and 10 h possessed a relative lower COF of 0.40–0.43. As a whole, the annealed coatings exhibited an equivalent COF of 0.40, which is much lower than that of as-sprayed coating (~0.79) at room temperature.

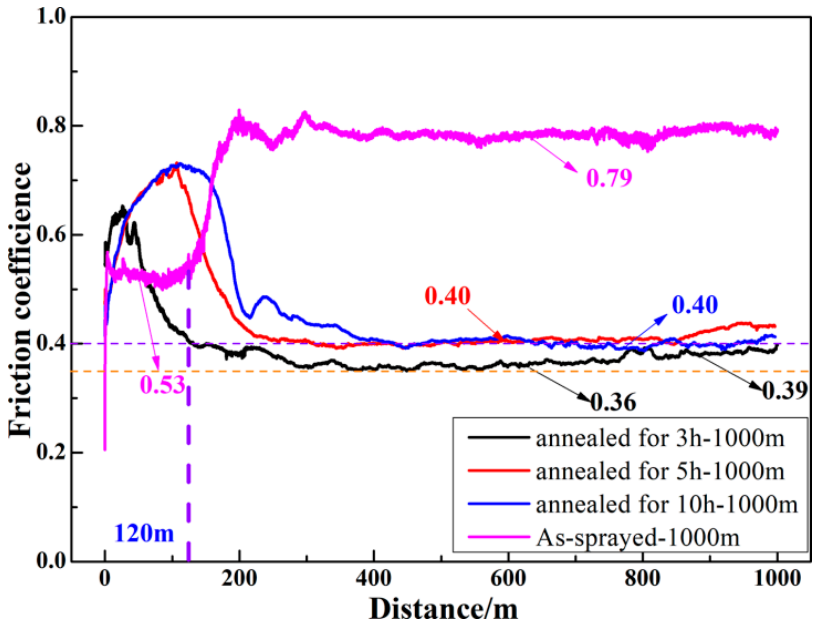

Figure 8. Friction coefficient–distance curves of as-sprayed and annealed CoMoCrSi coatings.

Figure 9 displays the wear rates of as-sprayed and annealed CoMoCrSi coatings. It is obvious that as-sprayed coating processes the highest wear rate of 9.169 × 10^{-6} $mm^3 \cdot N^{-1} \cdot m^{-1}$ at RT, however, the wear rates of annealed coatings dropped one order of magnitude after the friction test. Specifically, the annealed coatings registered the wear rate of 0.878–0.719 × 10^{-6} $mm^3 \cdot N^{-1} \cdot m^{-1}$ after a sliding distance of 1000 m, which is superior to that of previous reports [12,29]. In addition, the cross-sectional profiles of the wear tracks of as-sprayed and annealed CoMoCrSi coatings (Figure 10) could further illustrate the differences in the wear extent—especially the width and depth of wear track for as-sprayed coatings, which were up to 430 μm and 5000 nm. However, the width of wear track for annealed coatings were about 280 μm and the depth was just about 800 nm. It could be also concluded that the improvement in microstructure and microhardness would lead to the significant enhancement of anti-wear properties, and that the lubricating phases formed on the annealed coatings surface reduce the friction during the sliding process.

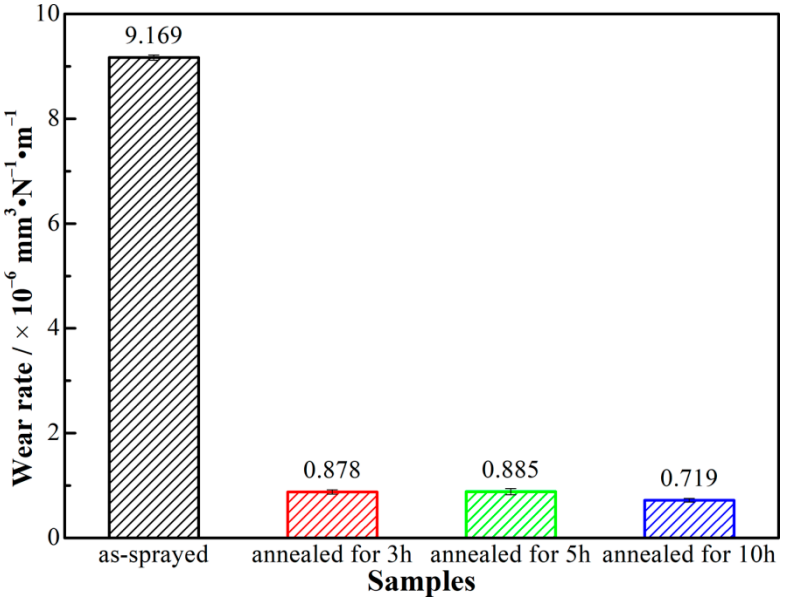

Figure 9. Wear rate of as-sprayed and annealed CoMoCrSi coatings.

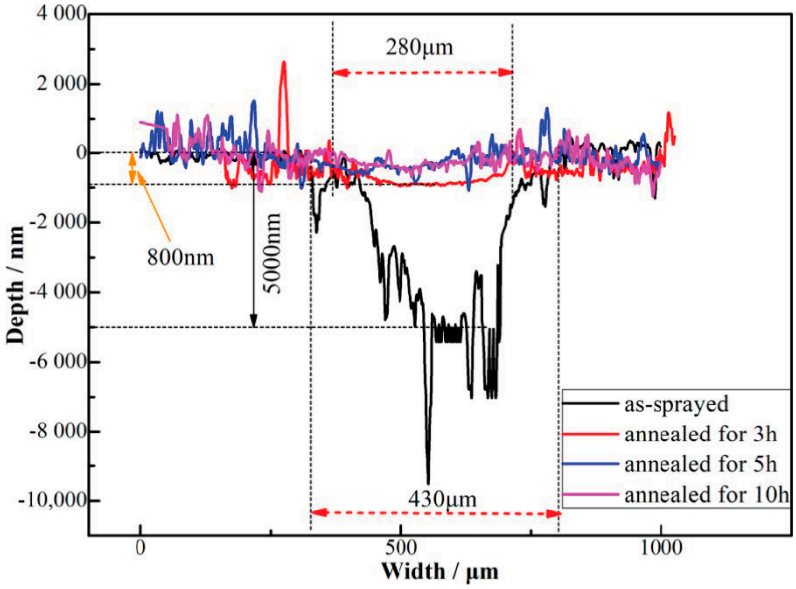

Figure 10. Cross-sectional profiles of the wear tracks after a sliding distance of 1000 m.

3.4. Discussion

To explore the causes of increased hardness, cross-sectional morphologies of annealed CoMoCrSi coatings were further investigated, as shown in Figure 11. A compact oxides layer in the range of 630 to 1150 nm can be seen, the thickness of which increased with increasing annealing time. Furthermore, the element-mapping result shows that the nano-sized oxides layer is enriched in Cr and O elements, as indicated in Figure 12. It should be noted that the coating annealed for 3 h was selected as a representative. In combination with the above statement, the oxide layer (at this position) mainly consisted of Cr_2O_3. It is interesting that the amount of Cr was lower in the coating part and present on the coating surface, and the Si either agglomerated at the bottom of oxides layer or intensively distributed in the coating. It could be concluded that the Cr and Si elements stopped further migration of other elements during the heat treatment. Moreover, both elements play a dual role of prohibiting the permeation of the O element from atmosphere and further serious oxidation of the coating. It is worth noting that the oxidation mechanism in present work was different to that of the solid T-800alloy [14], where the outermost Co_3O_4 layer was followed by some $CoMoO_4$ after exposure oxidation at 800 °C for 40 h, and the non-protective external scale could not prevent the dissolution of oxygen in the substrate alloy. This might be on account of the different fabrication process and status of the material. A conclusion could be drawn as that the high hard oxide layer on the coatings surfaces resisted indentation during the hardness test and this accounted for increased surface microhardness, which would also play a critical role of improving anti-wear performance during the sliding process.

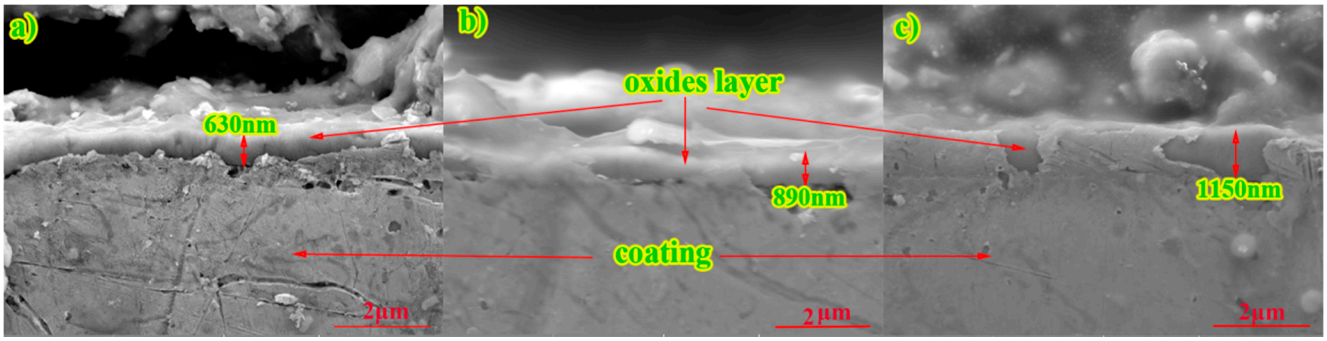

Figure 11. The cross-sectional images of oxides layer of CoMoCrSi coatings annealed for 3 h (**a**), 5 h (**b**), and 10 h (**c**).

Figure 13 illustrates the worn surface of as-sprayed and annealed CoMoCrSi coatings after a sliding distance of 1000 m. It is obvious that as-sprayed and annealed coatings registered different wear mechanism. Specifically, there are numerous brittle failure and friction scratches as well as some flat surface on the wear track of as-sprayed coating. Further investigation displayed that the brittle failure area was rich in Co, Mo, Cr, and O, demonstrating that wear debris are formed by the rolling compaction of counterparts during the sliding process (as indicated in Figure 13a), and it is easier for the tiny debris to capture the O element. Moreover, the flat areas are richer in element Cr, Mo, and Co, implying this part has not been crushed. Additionally, friction scratch areas exhibit a large number of fish scales (as shown in insert in Figure 13a), demonstrating serious scraping occurred during the friction process. These areas are rich in Co, Mo and O, according to the EDS result. This might be the result of easier oxidation occurring on the freshly-scratched surface of Co–Mo alloys. As the friction process continues, the coating will continue its brittle failure and become wear debris, and the wear in the fish-scale areas will also increase, eventually leading to a higher wear rate and larger depth of wear track (as indicated in Figures 9 and 10). It could be concluded that a brittle fracture coupled with abrasive wear dominated in the wear mechanism of as-sprayed coating at RT.

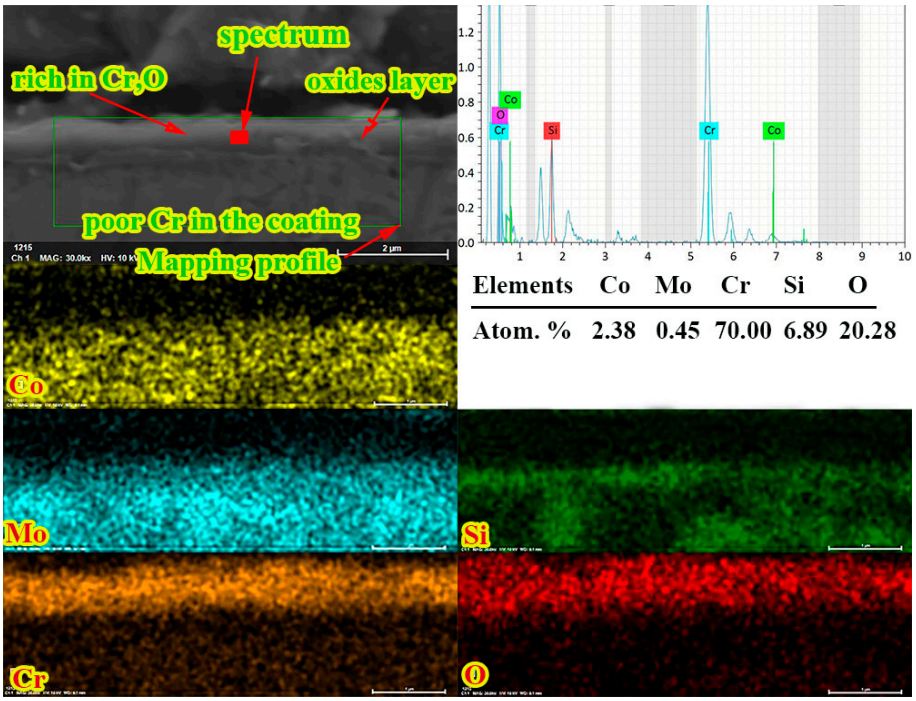

Figure 12. Elemental maps of oxides layer of CoMoCrSi coatings annealed for 3 h.

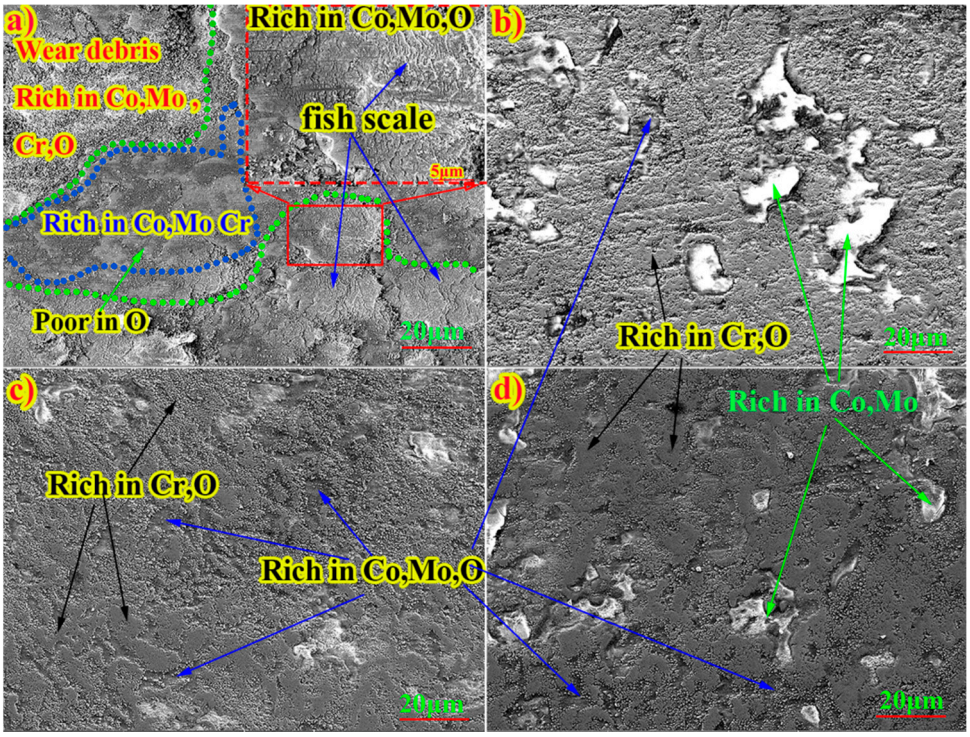

Figure 13. Worn surface of as-sprayed CoMoCrSi coatings (**a**) and coatings annealed for 3 h (**b**), 5 h (**c**), and 10 h (**d**).

As for the annealed coatings, the worn surfaces were relatively flatter compared to that of the as-sprayed coating. In particular, numerous white light areas (rich in Co and Mo) and dark grey areas (rich in Co, Mo, and O) were distributed on the grey worn surface (rich in Cr and O), as shown in Figure 13b–d. Figure 14 demonstrates elemental maps of worn surface of the coating annealed for 5 h, which could well verify the above conclusion. In the top insert in Figure 14, the particle areas show obvious sign of worn Cr_2O_3 particles,

indicating that Cr_2O_3 particles play an anti-wear role during the friction process. The smooth, dark, and compact island areas are rich in Co, Mo, and O, demonstrating the existence of $CoMoO_4$, which could play the critical role of lubrication [18]. As a result, annealed coatings exhibited lower COFs and wear rates. It must be noted that the small light areas displayed higher content of Co and Mo, and subtle cracks (as indicated in Figure 14), implying the existence of Co–Mo alloy, which well corresponds to the fish-scale pattern appearing on the wear surface of as-sprayed coating.

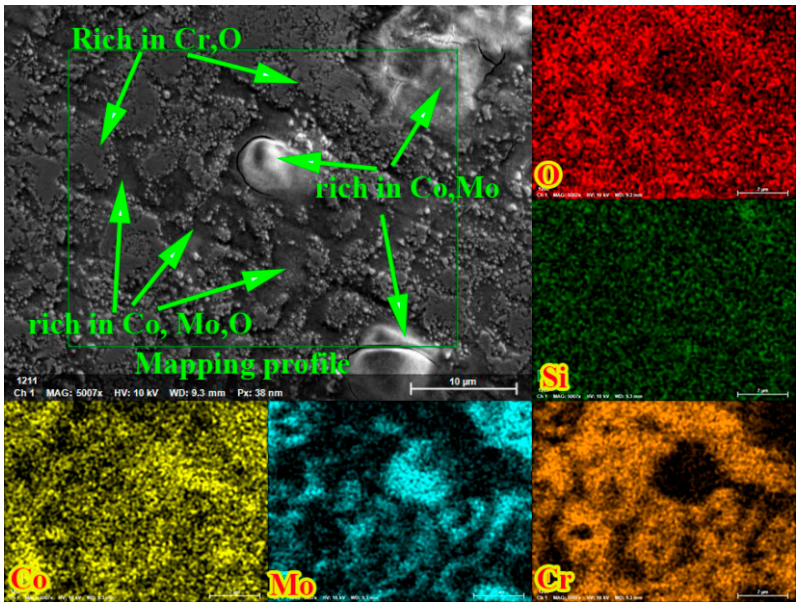

Figure 14. Elemental maps of worn surface of CoMoCrSi coating annealed for 5 h.

In addition, the results of Raman analysis (Figure 15) conducted on worn surfaces further confirmed the existence of MoO_3 (115, 144, 189, 238, and 665 cm^{-1}) [30–32], Co_3O_4 (194, 470, 488, 521, 618, and 691 cm^{-1}) [33,34], Cr_2O_3 (300, 332, 532, 551, 607, 685, and 700 cm^{-1}) [35,36], and $CoMoO_4$ (345, 367, 816, 876, and 937 cm^{-1}) [37,38]. In particular, the small number and weak intensities of the Cr_2O_3 peaks implies that they did not dominate on the worn surface of as-sprayed coating (Figure 15a). Furthermore, there was no lubricating $CoMoO_4$ in the wear track, resulting in high COF and wear rate. However, the Cr_2O_3 and $CoMoO_4$ dominated on the worn surface of annealed coating, and the content of Cr_2O_3 gradually increased when prolonging the annealing time, and $CoMoO_4$ phases reduced conversely. The increase of Cr_2O_3 and reduction of $CoMoO_4$ phases is well in accordance with above results and could account for the slight increase of COF while prolonging the annealing time. Irrespective of the cause, a dual coating of Cr_2O_3 and $CoMoO_4$ formed on the annealed coating surface might play a critical role in reducing friction and wear during the sliding process, and results in lowering COF and wear rates.

Another investigation was conducted on the worn surface of the coating annealed for 3 h with different sliding distances of 300, 500, and 1000 m, as shown in Figure 16. The process of wear can be seen from the images, and the wear degree of Cr_2O_3 particles increases with the sliding distance increase. Specifically, Figure 16a illustrates the rough surface and light wear of Cr_2O_3 particles, Figure 16b displays the polished state of Cr_2O_3 particles indicating further wear, and Figure 16c demonstrates the glazed surface of Cr_2O_3 particles. Furthermore, the element distribution on the worn Al_2O_3 pair vs. the coating annealed for 3 h after a sliding distance of 500 m is depicted in Figure 17. Combined with the EDS result, the large high-brightness areas of Co and Mo elements on the transfer film demonstrate the most of the Co- (23.14 at.%) and Mo- (15.08 at.%) oxides were removed during friction, however, the low Cr content (2.42 at.%) on the transfer film implies Cr_2O_3 mainly existed in the wear track. That is, the Cr_2O_3 phases play a key role of anti-wear

during the friction process. It could be concluded that slight abrasive wear dominates in the wear mechanism of annealed coatings at RT.

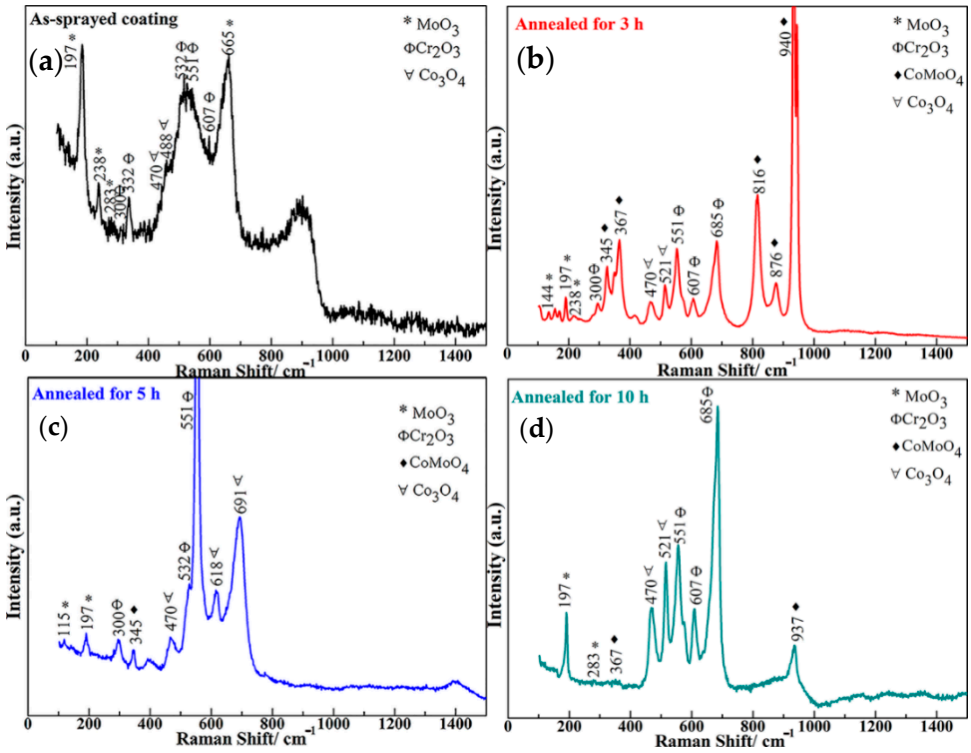

Figure 15. Raman patterns of the worn surfaces of as-sprayed CoMoCrSi coating (**a**) and coatings annealed for 3 h (**b**), 5 h (**c**), and10 h (**d**).

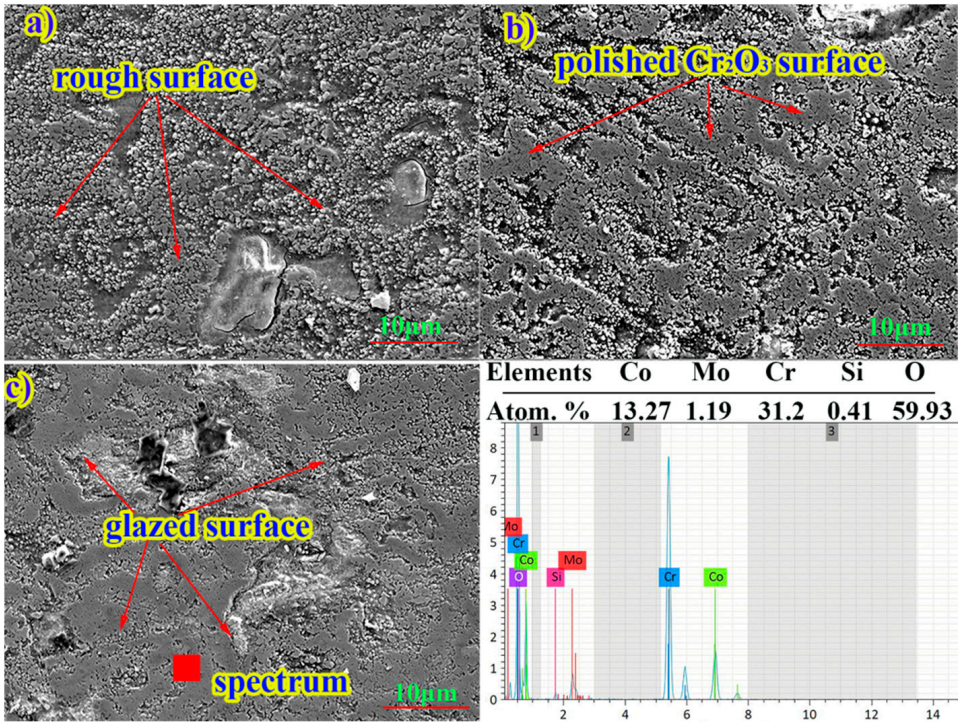

Figure 16. SEM images of the worn surfaces of CoMoCrSi coating annealed for 3 h with a distance of 300 m (**a**), 500 m (**b**), and 1000 m (**c**).

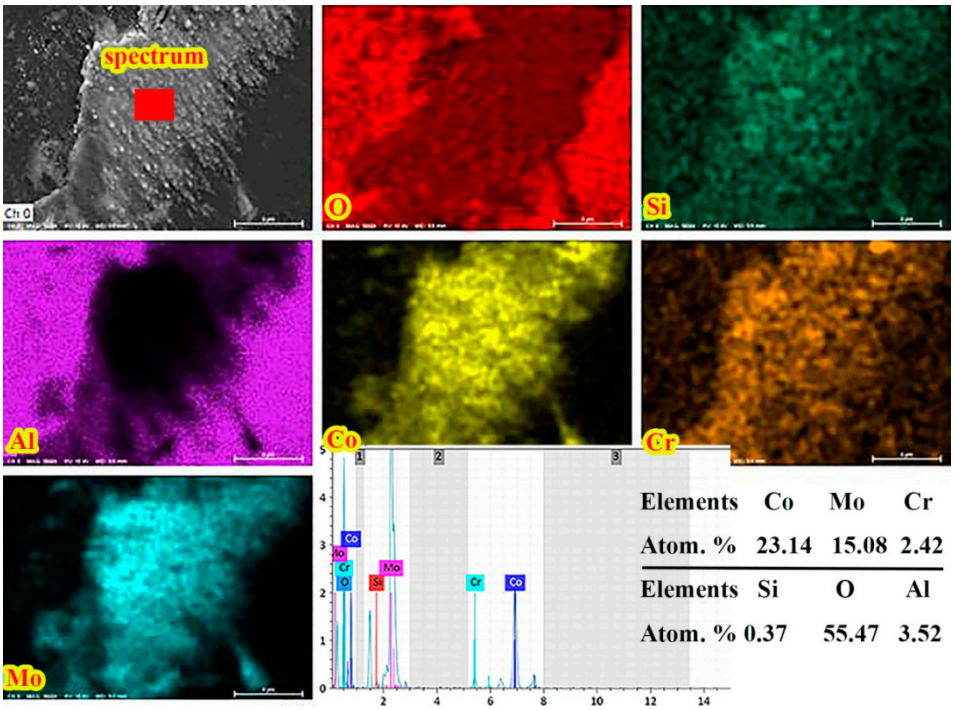

Figure 17. Elemental maps acquired from the worn surface of the Al_2O_3 pair for the coating annealed for 3 h after the sliding distance of 500 m.

4. Conclusions

In conclusion, the annealed treatment at 800 °C led to recrystallization, improved microstructures, and enhanced hardness of CoMoCrSi coatings. Most of all, the annealed coatings exhibited low COFs of 0.40 and wear rates of 0.7–0.8 × 10^{-6} $mm^3 \cdot N^{-1} \cdot m^{-1}$ after a long sliding distance of 1000 m, which were much lower than those of as-sprayed CoMoCrSi coating and other alloys at RT. In addition, an oxide layer formed on the annealed coating surfaces, which was mainly composed of micro-sized $CoMoO_4$ and nano-sized Cr_2O_3 and could have contributed to the increased surface microhardness (up to 1257.9 $HV_{0.3}$) and enhanced tribological performance of annealed coatings. In particular, the very hard Cr_2O_3 layer played the critical roles of resisting press-in and anti-wear during the tests, and the $CoMoO_4$ had a lubricating effect during the sliding process. Finally, the wear tracks of the annealed coatings indicated that the worn Cr_2O_3 particles were distributed in the soft Co–Mo–O or Co–Mo–Cr matrix after friction test. Consequently, the wear mechanism transferred from brittle fracture coupled with abrasive wear for the as-sprayed coating to slight abrasive wear for the annealed coatings. In view of the industrial applications, our results would not only enrich theoretical knowledge of heat treatment, but also furnish a technical reference for improving tribological performance of Co-based alloy coatings. Moreover, when we comprehensively considered the microhardness and tribological properties of the annealed coatings and the economic cost, the annealing time of 3 h was found to be the most appropriate.

Author Contributions: Writing—Review & editing, H.G.; Data curation, B.L. and Z.W.; Formal analysis, B.L.; Project administration, P.Y. All authors have read and agreed to the published version of the manuscript.

Funding: This research was funded by the National Natural Science Foundation of China (Grant Nos. 51665026, 51805408), the Outstanding Youth Foundation of Gansu Province (Grant No. 20JR5RA212), the "Light of West China" talent program of Chinese Academy of Sciences, the China Postdoctoral Science Foundation (Grant Nos. 2019M663851, 2019M653597), the Young Science and Technology Foundation of Gansu Academy of Sciences (Grant No. 2019QN-07), and Doctoral start-up funds (Grant No. LZCU-BS2019-29).

Institutional Review Board Statement: All affiliations agree to publish the paper.

Informed Consent Statement: All authors agree to publish the paper.

Data Availability Statement: The data is true and reliable.

Acknowledgments: The authors gratefully acknowledge the National Natural Science Foundation of China (Grant Nos. 51665026, 51805408), the Outstanding Youth Foundation of Gansu Province (Grant No. 20JR5RA212), the "Light of West China" talent program of Chinese Academy of Sciences, the China Postdoctoral Science Foundation (Grant Nos. 2019M663851, 2019M653597), the Young Science and Technology Foundation of Gansu Academy of Sciences (Grant No. 2019QN-07), and Doctoral start-up funds (Grant No. LZCU-BS2019-29) for their financial support. The authors also appreciate the constructive comments from the reviewers.

Conflicts of Interest: The authors declare no conflict of interest.

References

1. Vaßen, R.; Kaßner, H.; Stuke, A.; Hauler, F.; Hathiramani, D.; Stoever, D. Advanced thermal spray technologies for applications in energy systems. *Surf. Coat. Technol.* **2008**, *202*, 4432–4437. [CrossRef]
2. Wang, Y.; Stella, J.; Darut, G.; Poirier, T.; Liao, H.; Planche, M.-P. Aps Prepared NiCrBSi -YSZ Composite Coatings for Protection against Cavitation Erosion. *J. Alloys Compd.* **2017**, *699*, 1095–1103. [CrossRef]
3. Liu, L.; Xu, H.; Xiao, J.; Wei, X.; Zhang, G.; Zhang, C. Effect of heat treatment on structure and property evolutions of atmospheric plasma sprayed NiCrBSi coatings. *Surf. Coat. Technol.* **2017**, *325*, 548–554. [CrossRef]
4. Chen, Y.; Zhao, X.; Dang, Y.; Xiao, P.; Curry, N.; Markocsan, N.; Nylén, P. Characterization and understanding of residual stresses in a NiCoCrAlY bond coat for thermal barrier coating application. *Acta Mater.* **2015**, *94*, 1–14. [CrossRef]
5. Koiprasert, H.; Dumrongrattana, S.; Niranatlumpong, P. Thermally sprayed coatings for protection of fretting wear in land-based gas-turbine engine. *Wear* **2004**, *257*, 1–7. [CrossRef]
6. De Lacalle, L.N.L.; Gutiérrez, A.; Lamikiz, A.; Fernandes, M.H.; Sánchez, J.A. Turning of Thick Thermal Spray Coatings. *J. Therm. Spray Technol.* **2001**, *10*, 249–254. [CrossRef]
7. Liu, E.; Zhang, J.; Chen, S.; Du, S.; Du, L.; Cai, H.; Wang, L. High temperature negative wear behaviour of VN/Ag composites induced by expansive oxidation reaction. *Ceram. Int.* **2021**. [CrossRef]
8. Kowalski, S. Assessment of the Possibility of the Application of a CrN+OX Multi-Layer Coating to Mitigate the Development of Fretting Wear in a Press-Fit Joint. *Wear* **2018**, *398*, 13–21. [CrossRef]
9. Kowalski, S.; Cygnar, M.; Cieślikowski, B. Analysis of the application of ZrN coatings for the mitigation of the development of fretting wear processes at the surfaces of push fit joint elements. *Proc. Inst. Mech. Eng. Part J J. Eng. Tribol.* **2020**, *234*, 1208–1221. [CrossRef]
10. Kowalski, S. The influence of selected PVD coatings on fretting wear in a clamped joint based on the example of a rail vehicle wheel set. *Eksploatacja i Niezawodnosc Maint. Reliab.* **2018**, *20*, 1–8. [CrossRef]
11. Shukla, V.N.; Jayaganthan, R.; Tewari, V.K. Degradation Behavior of HVOF-Sprayed Cr_3C_2-25%NiCr Cermet Coatings Exposed to High Temperature Environment. *Mater. Today Proc.* **2015**, *2*, 1805–1813. [CrossRef]
12. Bolelli, G.; Lusvarghi, L. Tribological properties of HVOF as-sprayed and heat treated Co–Mo–Cr–Si coatings. *Tribol. Lett.* **2006**, *25*, 43–54. [CrossRef]
13. Zhang, X.H.; Zhang, C.; Zhang, Y.D.; Salam, S.; Wang, H.F.; Yang, Z.G. Effect of yttrium and aluminum additions on isothermal oxidation behavior of Tribaloy T-700 alloys. *Corros. Sci.* **2014**, *88*, 405–415. [CrossRef]
14. Zhang, Y.D.; Yang, Z.G.; Zhang, C.; Lan, H. Oxidation Behavior of Tribaloy T-800 Alloy at 800 °C and 1000 °C. *Oxid. Met.* **2008**, *70*, 229–239. [CrossRef]
15. Zhang, Y.D.; Zhang, C.; Lan, H.; Hou, P.Y.; Yang, Z.G. Improvement of the oxidation resistance of Tribaloy T-800 alloy by the additions of yttrium and aluminium. *Corros. Sci.* **2011**, *53*, 1035–1043. [CrossRef]
16. Cho, J.Y.; Zhang, S.H.; Cho, T.Y.; Yoon, J.H.; Joo, Y.K.; Hur, S.K. The processing optimization and property evaluations of HVOF Co-base alloy T800 coating. *J. Mater. Sci.* **2009**, *44*, 6348–6355. [CrossRef]
17. Yang, W.; Zou, L.; Cao, X.; Liu, J.; Li, D.; Cai, Z. Fretting wear properties of HVOF-sprayed CoMoCrSi coatings with different spraying parameters. *Surf. Coat. Technol.* **2019**, *358*, 994–1005. [CrossRef]
18. Guo, H.; Wang, Y.; Hao, E.; Li, B.; An, Y.; Chen, J.; Zhou, H.; Yan, P.; Wu, Z. CoMoCrSi coatings prepared by high-velocity oxygen fuel spraying: Microstructure and mechanical properties at elevated temperatures up to 800 °C. *Mater. Res. Express* **2020**, *6*, 1265e9. [CrossRef]
19. Li, B.; Gao, Y.; Jia, J.; Han, M.; Guo, H.; Wang, W. Influence of heat treatments on the microstructure as well as mechanical and tribological properties of NiCrAlY-Mo-Ag coatings. *J. Alloy. Compd.* **2016**, *686*, 503–510. [CrossRef]
20. Chen, L.-Y.; Xu, T.; Lu, S.; Wang, Z.-X.; Chen, S.; Zhang, L.-C. Improved hardness and wear resistance of plasma sprayed nanostructured NiCrBSi coating via short-time heat treatment. *Surf. Coat. Technol.* **2018**, *350*, 436–444. [CrossRef]
21. Salehi Doolabi, D.; Rahimipour, M.R.; Alizadeh, M.; Pouladi, S.; Hadavi, S.M.M.; Vaezi, M.R. Effect of high vacuum heat treatment on microstructure and cyclic oxidation resistance of HVOF-CoNiCrAlY coatings. *Vacuum* **2017**, *135*, 22–33. [CrossRef]

22. Houdková, Š.; Smazalová, E.; Pala, Z. Effect of Heat Treatment on the Microstructure and Properties of HVOF-Sprayed Co-Cr-W Coating. *J. Therm. Spray Technol.* **2015**, *25*, 546–557. [CrossRef]
23. Wang, Y.; Liu, J.; Kang, N.; Darut, G.; Poirier, T.; Stella, J.; Liao, H.; Planche, M.-P. Cavitation erosion of plasma-sprayed CoMoCrSi coatings. *Tribol. Int.* **2016**, *102*, 429–435. [CrossRef]
24. Bolelli, G.; Lusvarghi, L. Heat Treatment Effects on the Tribological Performance of HVOF Sprayed Co-Mo-Cr-Si Coatings. *J. Therm. Spray Technol.* **2006**, *15*, 802–810. [CrossRef]
25. Tang, L.; He, P.; Kang, J.; Wang, L.; Ding, S.; Chen, S.; Zhu, X.; Xie, F.; Zhou, L.; Ma, G.; et al. Significantly enhanced mechanical and tribological properties of Co-based alloy coatings by annealing treatment. *Tribol. Int.* **2020**, *146*, 106265. [CrossRef]
26. Lin, C.; Yen, S.; Su, C. Measurement and optimization of atmospheric plasma sprayed CoMoCrSi coatings parameters on Ti-6Al-4V substrates affecting microstructural and properties using hybrid abductor induction mechanism. *Measurement* **2016**, *94*, 157–167. [CrossRef]
27. Henriques, B.; Faria, S.; Soares, D.; Silva, F.S. Hot pressing effect on the shear bond strength of dental porcelain to CoCrMoSi alloy substrates with different surface treatments. *Mater. Sci. Eng. C* **2013**, *33*, 557–563. [CrossRef] [PubMed]
28. Prasad, C.D.; Joladarashi, S.; Ramesh, M.R.; Srinath, M.S.; Channabasappa, B.H. Effect of microwave heating on microstructure and elevated temperature adhesive wear behavior of HVOF deposited CoMoCrSi-Cr_3C_2 coating. *Surf. Coat. Technol.* **2019**, *374*, 291–304. [CrossRef]
29. Navas, C.; Cadenas, M.; Cuetos, J.M.; de Damborenea, J. Microstructure and sliding wear behaviour of Tribaloy T-800 coatings deposited by laser cladding. *Wear* **2006**, *260*, 838–846. [CrossRef]
30. Wang, K.; Wang, F.; Liu, Y.; Pan, G. Vapor growth and photoconductive property of single-crystalline MoO3 nanosheets. *Mater. Lett.* **2013**, *102–103*, 8–11. [CrossRef]
31. Sun, H.; Zhang, H.; Jing, X.; Hu, J.; Shen, K.; Liang, Z.; Hu, J.; Tian, Q.; Luo, M.; Zhu, Z.; et al. One-step synthesis of centimeter-size alpha-MoO_3 with single crystallinity. *Appl. Surf. Sci.* **2019**, *476*, 789–795. [CrossRef]
32. Chandoul, F.; Boukhachem, A.; Hosni, F.; Moussa, H.; Fayache, M.S.; Amlouk, M.; Schneider, R. Change of the properties of nanostructured MoO 3 thin films using gamma-ray irradiation. *Ceram. Int.* **2018**, *44*, 12483–12490. [CrossRef]
33. Olejníček, J.; Šmíd, J.; Perekrestov, R.; Kšírová, P.; Rathouský, J.; Kohout, M.; Dvořáková, M.; Kment, Š.; Jurek, K.; Čada, M.; et al. Co_3O_4 thin films prepared by hollow cathode discharge. *Surf. Coat. Technol.* **2019**, *366*, 303–310. [CrossRef]
34. Hadjiev, V.G.; Iliev, M.N.; Vergilov, I.V. The Raman spectra of Co_3O_4. *J. Phys. C Solid State Phys.* **1988**, *21*, L199–L201. [CrossRef]
35. Roy, M.; Ghosh, S.; Naskar, M.K. Solvothermal synthesis of Cr_2O_3 nanocubes via template-free route. *Mater. Chem. Phys.* **2015**, *159*, 101–106. [CrossRef]
36. Fleischer, K.; Caffrey, D.; Farrell, L.; Norton, E.; Mullarkey, D.; Arca, E.; Shvets, I.V. Raman spectra of p-type transparent semiconducting Cr_2O_3:Mg. *Thin Solid Films* **2015**, *594*, 245–249. [CrossRef]
37. Yang, T.; Zhang, H.; Luo, Y.; Mei, L.; Guo, D.; Li, Q.; Wang, T. Enhanced electrochemical performance of $CoMoO_4$ nanorods/reduced graphene oxide as anode material for lithium-ion batteries. *Electrochim. Acta* **2015**, *158*, 327–332. [CrossRef]
38. Jiang, G.; Li, L.; Huang, Z.; Xie, Z.; Cao, B. Rod-like porous $CoMoO_4$@C as excellent anode for high performance lithium ion battery. *J. Alloys Compd.* **2019**, *790*, 891–899. [CrossRef]